ACS OMEGA

http://pubs.acs.org/journal/acsodf

Article

Nanocomposite of CO_2-Based Polycarbonate Polyol with Highly Exfoliated Nanoclay

Mohammad Alroaithi* and Wei Xu

Cite This: *ACS Omega* 2023, 8, 5247−5256

Read Online

ACCESS | Metrics & More | Article Recommendations

ABSTRACT: Polypropylene carbonate (PPC) derived from carbon dioxide has been used as a precursor for the synthesis of polyurethane (PU). The high viscosity of the PPC is the key parameter hindering its processability during PU synthesis. Herein, a PPC nanocomposite with highly exfoliated nanoclay was prepared through a solution intercalation process. A wide range of nanoclay concentrations incorporated into the PPC were studied. The impacts of the nanoclay on the PPC were investigated in order to maintain the polymer structure while improving its physical properties. The characterizations of PPC nanocomposites showed that the highly exfoliated nanoclay contributed to a viscosity reduction, and a slight reduction in the molecular weight. The polymer degradation was indicated by the formation of cyclic propylene carbonate. The minimum or critical concentration of nanoclay was found to be between ∼0.5 and 2.0 wt %. Within this range, the polymer degradation is minimal. The PPC nanocomposites with a lower viscosity showed excellent precursors for making PU coating materials. The PU coating derived from the PPC nanocomposite has higher anticorrosive properties in comparison with the non-modified PU coating.

INTRODUCTION

Concerns over carbon dioxide (CO_2) emissions have prompted more research and development into the use of CO_2 for value-added materials.[1−3] CO_2 is a renewable and low-cost feedstock that can be used as a primary component for the production of biodegradable and biocompatible CO_2-based polymers.[4,5] CO_2-based polymers exhibit some distinctive characteristic features, including lower production costs, sequestering up to 52% CO_2 in polymer backbones and improved physical properties over other conventional purely hydrocarbon-based polymers.[6−9]

CO_2-based polycarbonate polyols [i.e., polypropylene carbonate, (PPC), and polyethylene carbonate] are examples of versatile products that can be derived from the copolymerization of CO_2 with epoxides such as propylene oxide or ethylene oxide.[10,11] The PPC polyols have found applications in elastomers, coatings, foams, adhesives, and as additives in the oil field.[12−14] However, PPC polyols suffer from a lower thermal degradation temperature, poorer mechanical strength, and higher viscosity, which result in inferior performance and processability.[15]

Polymer-based nanocomposites have recently attracted intensive research interest owing to their promising potential for improving the physical properties of a polymer.[16−20] A polymer nanocomposite is a type of material that incorporates one or more nanofillers into a polymer matrix.[21,22] The homogeneous dispersion and the chemical compatibility between the polymer matrix and nanofillers are of critical factors for the polymer nanocomposites synthesis and their properties enhancements.[23−28] The importance of nanoclay-based polymer nanocomposites has been found in various applications, including membrane separation,[29] coating,[30] drug delivery,[31] adsorption for CO_2,[32] and wastewater treatment.[33,34]

Montmorillonite (MMT) is an inorganic nanofiller, made of layered silicates, that is widely used for polymer nanocomposite synthesis. MMT has several advantages including high surface area, low cost, high degree of intercalation and exfoliation as well as superior enhancement in the resulting properties of polymer nanocomposites.[35] The inorganic cation of Na^+—MMT is usually exchanged with an organic cation such as $[R_4N]^+$ in order to change the hydrophilic nature of MMT nanoclay to hydrophobic. This makes the organic polymer chain to be homogeneously hosted between the nanoclay layers.

Polymer nanocomposites containing MMT nanoclay can be formed in different structures depending on the used preparation method such as phase separation, intercalated structures, and/or an exfoliated structures.[36] In the phase separation, the polymer is separated from the nanoclay as a result of poor dispersion and/or nanoclay aggregation.[37] An intercalated structure, on the other hand, occurs when the

Received: September 2, 2022
Accepted: December 7, 2022
Published: February 1, 2023

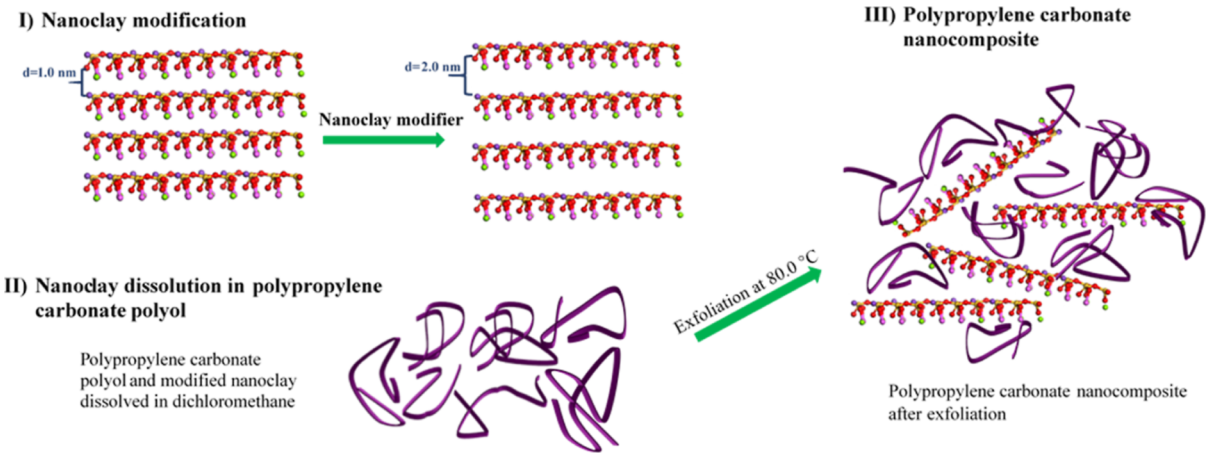

Figure 1. Schematic illustration for the preparation of PPC nanocomposites. Stage I: modification of nanoclay with 25.0−30.0 wt % trimethyl stearyl ammonium. The modification doubles the d-spacing. Stage II: dissolving of the PPC polyol and modified nanoclay in the solvent of dichloromethane. Stage III: nanoclay exfoliation in polymer at T = 80.0 °C, and the formation of PPC nanocomposites after exfoliation.

polymer chains intercalate between the nanoclay layers, altering their interlayer spacing until a point where the electrostatic forces between the nanoclay layers are diminished, causing a fully separated nanoclay stack (exfoliated structure).[38] The polymer nanocomposites can be synthesized through different routes, including melt-blending, in situ polymerization and solution intercalation (solvent-based). The latter one is considered to be the method of choice due to the favorable dispersion of nanoclay within the polymer matrix.[39]

In this study, the use of a low-molecular-weight CO_2-based polycarbonate polyol (PPC) for preparing nanocomposites was explored for the first time. The PPC polyol nanocomposites were prepared through a solution intercalation route using a MMT nanoclay. A wide range of nanoclay concentrations, incorporated into PPC polyols were studied. The molecular weight and the polymer degradation of the PPC polyol nanocomposites were monitored in order to maintain the polymer structure while improving their physical properties. The developed PPC polyol nanocomposites were extended to produce polyurethane (PU)-based coating materials. The anticorrosion properties of PU coating were also studied.

EXPERIMENTAL SECTION

Materials. CO_2-based polycarbonate polyol (PPC) with a number-average molecular weight (M_n) of ∼1000 g mol^{-1} was provided by Aramco Performance Material, USA. MMT nanoclay, modified with 25.0−30.0 wt % trimethyl stearyl ammonium, and dichloromethane were purchased from Sigma-Aldrich and used as received without any further treatments.

Synthesis of PPC Nanocomposites. The PPC nanocomposites were prepared by a solution intercalation method.[39] Typically, 40.0 g of PPC polyol was dissolved in 160.0 mL of dichloromethane and stirred at room temperature until a homogeneous solution was obtained. A predetermined amount of the modified MMT nanoclay (0.5−8.0 wt %) was then added to the solution and stirred at 800 rpm. The reaction was performed in a three-necked flask equipped with a magnetic stirrer, condenser, and thermometer. The reaction was carried out under nitrogen at 80 °C for 5 h to ensure complete exfoliation. The mixture was then placed in a rotary evaporator at T = 80.0 °C for 1.0 h to remove the solvent. A sample was taken to carry out the analysis. The schematic illustration for the preparation of CO_2-based polycarbonate polyol nanocomposites is shown in Figure 1.

Synthesis of PU Coating from PPC Polyol Nanocomposite. The developed PPC nanocomposites were used to produce PU-based coating materials. The PU coating was prepared through a two-step reaction. In the first step, the isocyanate end-capped prepolymer was prepared by adding 8.0% methylene diphenyl diisocyanate to the flask containing the PPC nanocomposite. The reaction was carried out at 90 °C for 6 h under nitrogen purging.

In the second step, using the Doctor blade coating technique to control the thickness, the isocyanate end-capped prepolymer was transferred in front of the blade at a fixed distance from the surface (metal substrate) that needs to be covered. The blade is moved across in-line with the surface, creating a wet film of a predetermined thickness. The coated metal substrate is placed in an environmental chamber at 60 °C and 60% relative humidity for 24 h to ensure that fully curing were achieved.

Characterizations. *X-ray Diffraction.* An X-ray diffraction (XRD) analysis was performed on the Rigaku miniflex 600. The diffractometer was operated at 200 mA and 40 kV at ambient temperature. The scanning angle (2θ) covers a range from 2 to 15° at the scanning rate and speed step of 3° min^{-1} and 0.02°, respectively.

Chemical Structure. The chemical structures of the PPC polyols and their nanocomposites were analyzed by proton nuclear magnetic resonance spectroscopy (^{1}H NMR) using Bruker 400 MHz in deuterated chloroform at room temperature.

A Fourier transform infrared (FT-IR) spectra study was performed, using Thermo Nicolet is50R FT-IR in order to confirm the successful preparation of the nanocomposites. The samples were scanned from 4000 to 500 cm^{-1} with a resolution of 2 cm^{-1} and 32 scans.

Molecular Weight. The molecular weight and molecular weight distribution of PPC polyol and its nanocomposites were determined by gel permeation chromatography (GPC). Typically, 10.0 mg/mL was dissolved in a mobile phase containing 0.1% formic acid in tetrahydrofuran (THF). The polymer solution was passed through two GPC columns in series-Agilent MesoPore (300 × 7.5 mm) at a flow rate of 1.0 mL min^{-1}. Using the Cirrus GPC data analysis tool, the

https://doi.org/10.1021/acsomega.2c05705
ACS Omega 2023, 8, 5247−5256

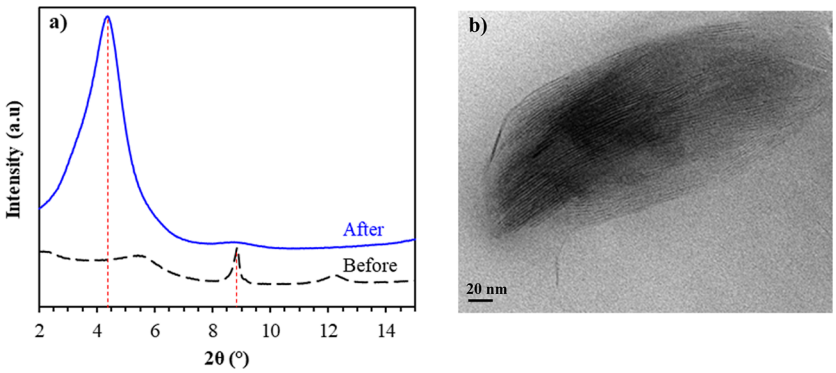

Figure 2. (a) XRD patterns of MMT nanoclay before and after surface modification with 25.0−30.0 wt % trimethyl stearyl ammonium. (b) TEM image of modified nanoclay before exfoliation with PPC polyol.

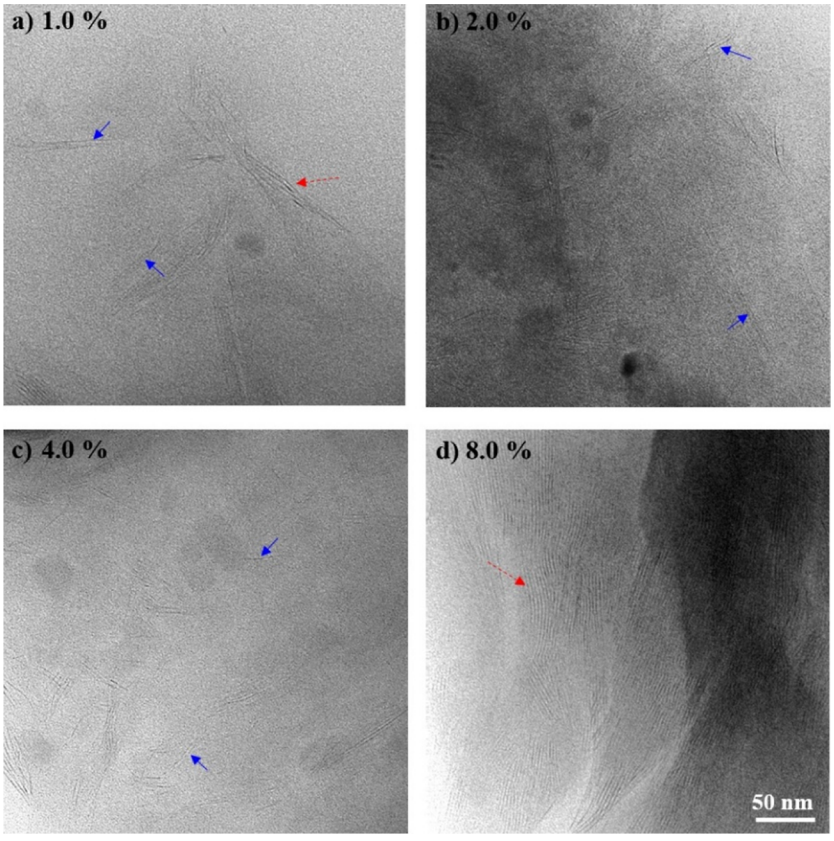

Figure 3. (a−d) TEM micrographs of PPC nanocomposites in the presence of various nanoclay concentrations.

molecular weight was obtained from a calibration curve of 11 narrow M_w of polystyrene standards.

Bruker Autoflex III matrix-assisted laser desorption ionization time-of-flight mass spectroscopy (MALDI−TOF−MS) was used to acquire mass spectral data. The sample was dissolved in THF with dithranol as the matrix and sodium trifluoroacetate as the cation source. The mixture was placed on the MALDI target plate and four different points were taken for measurement. The spectra were recorded under reflection in the positive ion mode using an accelerating voltage of 20 kV.

Thermal Analysis. The thermal stability of the sample was measured by thermogravimetric analysis (TGA) on the TA instrument TGA 5500. The sample was placed on platinum pans and heated at a rate of 10.0 °C min^{-1} from 30.0 to 500 °C under the protection of nitrogen N_2.

The thermal properties and glass transition temperature (T_g) of the samples were also analyzed by differential scanning calorimetry (DSC) on TA instrument DSC250 in an N_2 environment. The sample with a nominal weight of about 10.0 mg was sealed in aluminum crucibles. The sample was first heated from −50.0 to 150.0 °C at a heating rate of 10.0 °C min^{-1}. The sample was then quenched to −50 °C at a rate of 10.0 °C min^{-1} and finally heated again to 150.0 °C from −50.0 °C at a heating rate of 10.0 °C min^{-1}. The T_g was extrapolated from the graph using the second heating run.

Rheology. The steady shear rheological characteristic was investigated with a controlled stress rotational rheometer AR1500ex (TA Instruments, New Castle, DE, USA). A Peltier plate and cover were used to maintain a temperature of 60 °C while acquiring the flow curves. The measurement was carried out with a plate and cone fixture, with a 20.0 mm diameter and

https://doi.org/10.1021/acsomega.2c05705
ACS Omega 2023, 8, 5247−5256

a 1° cone angle using a gap of 22.0 μm which is the cone truncation height.

Morphology. The morphology of the nanocomposite was detected by transmission electron microscopy (TEM; Nippon Denshi Co., Japan, 200 kV). Typically, a small quantity of sample was diluted in ethanol (~1% mass), placed on a 200 mesh carbon film supported by a copper grid, and allowed to dry at room temperature.

Corrosion Analysis. Electrochemical impedance spectroscopy (EIS) measurements were conducted to evaluate the coating efficiency using a Gamry Interface 1000. A frequency response analyzer was used in conjunction with a potentiostat/galvanostat to conduct the electrochemical measurements. The electrochemical cell setup consisted of three electrodes. The coated sample was the working electrode with an exposed surface area of 1 cm^2, a standard calomel reference electrode, and platinum counter electrode made up the remainder of the cell. The measurement frequency ranges from 0.01 Hz to 100 kHz across the coated sample. The equivalent system impedance was determined from the measured system response at each frequency.

RESULTS AND DISCUSSION

The incompatibility of hydrophobic polymer chains with hydrophilic nanoclay layers prevents a homogeneous dispersion of nanoclay within the polymer. This incompatibility weakens the interfacial interactions; thus, hinders the exfoliation and preparation of nanocomposites.[38−40] Therefore, the surface modification of nanoclay layers with hydrophobic agents, through a cation exchange process, not only increases the *d*-spacing but also promotes the polymer chain intercalation into the galleries during nanocomposite preparation.[40]

XRD is a useful technique to characterize the nanoclay structure and identify the change in the clay's interlayer *d*-spacing. The XRD analysis provides information based on Bragg's law $2d\sin(\theta) = \lambda$, where θ is the incident angle, λ is the wavelength of the incident X-ray beam, and d refers to the one interlayer spacing and one nanoclay layer (*d*-spacing).[37] Figure 2a shows the XRD patterns of the MMT nanoclay before and after modification with 25.0−30.0 wt % trimethyl stearyl ammonium. The neat MMT nanoclay exhibits a diffraction peak at $2\theta = 8.85°$ which corresponds to the *d*-spacing of 1.0 nm. The degree of layers expansion (*d*-spacing) after modification is evidenced by the shifting diffraction peak toward a smaller angel at $2\theta = 4.40°$ which doubled the *d*-spacing to ca. 2.0 nm.[41] The enlarged *d*-spacing value clearly suggests a successful intercalation of trimethyl stearyl ammonium within the nanoclay layers, as shown in the TEM micrograph in Figure 2b.

The representative TEM micrograph shown in Figure 3a−d can be taken as a definitive evidence for the formation of intercalated and/or exfoliated structures in the polymer matrix. From Figure 3a−c, one can clearly see both exfoliated morphology (blue arrow) and minor intercalated nanoclay layers (red-dotted arrow) were formed. The layered platelets are likely to exfoliate in the presence of a repulsive polymer matrix, particularly at low-molecular-weight polymers. On the contrary, in high-molecular-weight polymers, the nanoclay layers are trapped via percolation and/or entanglement of surrounding polymer chains. Having said that, this explanation may also be applied where a high nanoclay concentration is present in the system. As shown in Figure 3d, the layers appeared in the form of bundles (intercalated layers) with 8.0 wt % nanoclay, indicating that the exfoliation did not take place due to the entanglement of surrounding polymer chains as well as the agglomeration of the nanoclay layers.[28]

In order to understand the mechanism of the polymer−filler interaction and compatibility from the thermodynamics point of view, the Gibbs free energy change ($\Delta G°$, kJ mol^{-1}) of the nanocomposites composed of a change in both enthalpy ($\Delta H°$, kJ mol^{-1}) and entropy ($\Delta S°$, J K^{-1} mol^{-1}) at a reaction temperature (T, Kelvin)

$$\Delta G_P^\circ = \Delta H_P^\circ - T\Delta S_P^\circ \quad (1)$$

$$\Delta G_C^\circ = \Delta H_C^\circ - T\Delta S_C^\circ \quad (2)$$

where the subscripts P and C refer to the thermodynamic parameters of the polymer and nanoclay, respectively.

Therefore, the total free energy change of the system, S is given by

$$\Delta G_S^\circ = \Delta H_S^\circ - T\Delta S_S^\circ \quad (3)$$

$$\Delta G_S^\circ = \Delta H_S^\circ - T(\Delta S_P^\circ + \Delta S_C^\circ) \quad (4)$$

When the polymer chains enter into the gallery of the nanoclay, they reside in a restrained form (i.e., ΔS_P° is negative). In contrast, the gallery expansion caused by the polymer chains would shift the entropy change in the nanoclay, ΔS_C° toward a positive value. Hence, ΔG_S° value will be negative indicating that the most favorable interaction between the nanoclay and the polymer occurs when ΔH_S° and ΔS_S° is negative and positive, respectively.[43]

The $\Delta H°$ is calculated using Fowkes' equation below, where $\Delta H°$ is the enthalpy of interaction between the phases in the binary system (nanocomposites), and $\Delta\bar{\nu}$ is the shift peak position (corresponding to a functional or reactive group of the polymer that is involved in the interaction).

$$\Delta H^\circ = 0.236 \times \Delta\bar{\nu} \quad (5)$$

The equation mainly deals with the thermodynamic free energy of mixing, as explained above, as well as the change in IR peak position with the enthalpy of interaction between the two systems. FT-IR spectroscopy is a well-proven tool for determining the change in ΔH_S° of nanocomposites. The effects of nanoclay content on the formation of polymer nanocomposites and their properties, through the solution intercalation, were studied within a wide range at 0.0, 1.0, 2.0, and 4.0 wt %.[25]

Figure 4 shows FT-IR spectra of neat polymer and its nanocomposites at different nanoclay concentrations. The typical absorption peaks for −C═O, C−O, and −O−CO− are 1670−1700, 1220−1230, and 1040−1115 cm^{-1}, respectively. The absorption peak for C−O stretching vibration observed at 1227 cm^{-1} for the neat polymer slightly decreased with the increase in nanoclay content (Table 1).[42]

The shifting of the C−O stretching peak toward a lower wavenumber in nanocomposites indicates that some interactions must have taken place between the polymer and nanoclay. This may be attributed to the intermolecular hydrogen bond between the surface hydroxyl (OH) functional group of the nanoclay and the C−O group of the polymer.[36−38]

The chemical structure of PPC polyol was analyzed by ^1H NMR. The signals at 1.2−1.3 ppm represent the protons in the terminal CH_3 group. The signals at 4.8−5.0, 3.9−4.3, and 1.3−

https://doi.org/10.1021/acsomega.2c05705
ACS Omega 2023, 8, 5247−5256

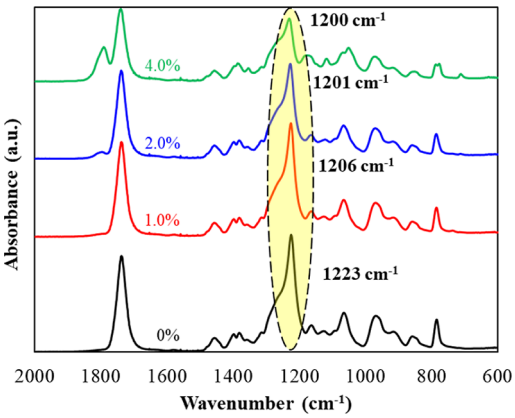

Figure 4. FT-IR spectrum of the neat PPC polyol and its nanocomposites with different nanoclay concentrations.

Table 1. Comparison of the Enthalpy and Its Energy Calculation of Various Nanocomposites

nanoclay content, wt %	peak position of C−O stretching, cm^{-1}	$\Delta\bar{\nu}$ of C−O, cm^{-1}	$\Delta H°$, k. cal. mol^{-1} for C−O
0	1223		
1	1206	17	−4.01
2	1201	22	−5.19
4	1200	23	−5.42

1.5 ppm in Figure 5a were assigned to the protons of CH, CH_2, and CH_3, respectively.[44]

The molecular weight of the PPC polyol value determined by MALDI−TOF−MS was 1000 g mol^{-1} (see Figure 5b). The result also exhibits a molecular weight difference of 102 g/mol (green arrow) between the peaks, which corresponds to the propylene carbonate units (see the chemical structure in Figure 5a). The molecular weight and its distribution were also confirmed by GPC analysis (Figure 5c) and the result was slightly higher than the corresponding value obtained by MALDI due to the different hydrodynamic volumes of the polystyrene standard employed for the GPC analysis.

To elucidate the effect of nanoclay content on the rheology of the polymer nanocomposites, the viscosity of all samples was measured at 60.0 °C as a function of the shear rate. The viscoelastic properties test provides us useful information on the phase behavior and physical interactions between the nanoclay and the polymer. From Figure 6a, one can observe a shear-thinning behavior of all samples, except for 8.0 wt %, and deviate with the increase in the nanoclay content. By increasing the nanoclay concentrations, up to 4.0 wt %, one can observe a viscosity reduction of the polymer nanocomposite. This result was unexpected because the literature reported that the nanofiller usually increases the viscosity of polymer nanocomposite due to intercalation/exfoliation achievement.[45] In our result, however, the high exfoliation degree of nanoclay lamellae has functioned as a plasticizer and caused a breakage in the chain entanglements. This will reduce the frication, and thus, increase the mobility of the polymeric chain (free volume of the polymer chain).[46−48]

However, this trend is shifted when a critical concentration, C_{cri}, is exceeded. When approaching the C_{cri}, a *U*-shape behavior in viscosity versus nanoclay concentrations was emerged. The reason for such a behavior beyond C_{cri} could be attributed to nanoclay coagulation, which limits the mobility of the polymer chains.[47,48] According to Figure 6a,b, the minimum viscosity obtained was 300 cP for 4.0 wt % nanoclay content, compared with 30000.0 cP for the neat PPC polyol.

In order to assess the effects of the addition of modified nanoclay on the thermal stability behavior of the PPC

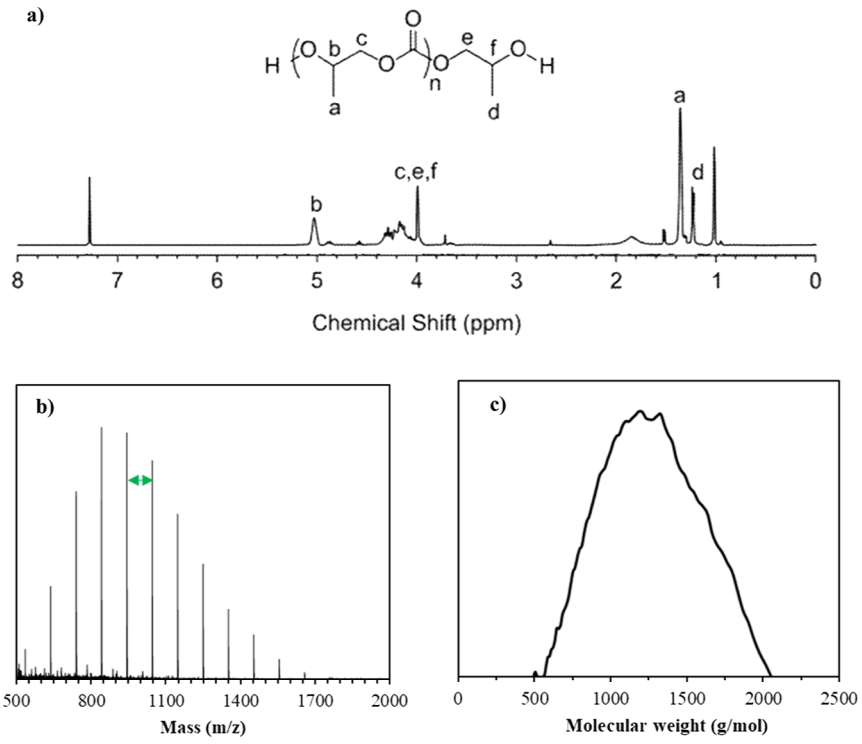

Figure 5. Characteristics of propylene carbonate polyol using (a) ^{1}H NMR spectrum and (b) MALDI−TOF−MS spectrum. (c) GPC.

https://doi.org/10.1021/acsomega.2c05705
ACS Omega 2023, 8, 5247−5256

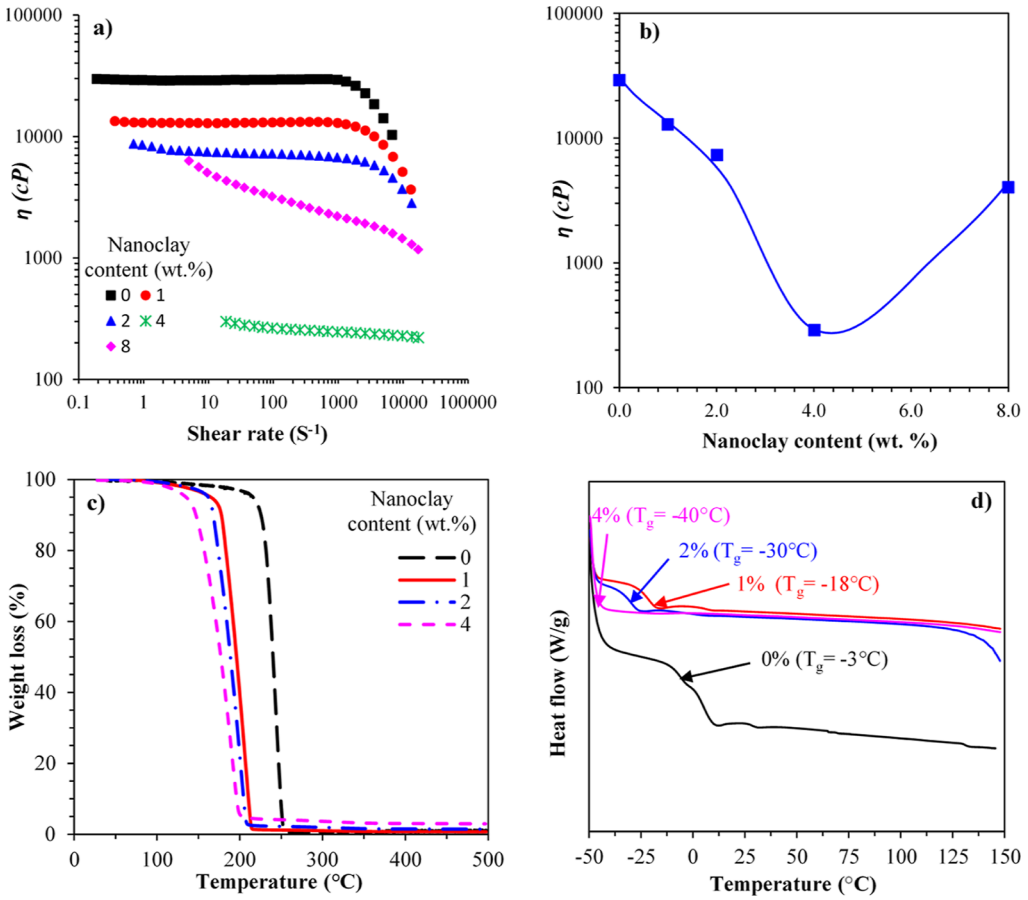

Figure 6. Viscosity of the polymer nanocomposites as a function of (a) shear rate; (b) nanoclay contents measured using oscillatory at a shear rate of 100 s^{-1} and at T = 60.0 °C. (c,d) TGA and DSC plot of polymer nanocomposites in the presence of various amounts of nanoclay concentrations, respectively.

nanocomposites, TGA studies have been carried out, and the results are presented in Figure 6c. From the TGA plot, one can see that the degradation temperature, T_d decreased with the increase in nanoclay concentration. With only 1.0 wt % nanoclay added to the polymer matrix, thermal stability dropped from 225 to 165 °C for the neat and 40.0 wt % PPC polyol, respectively. The thermal behavior beyond the addition of 1.0 wt % nanoclay did not exhibit to a major change.

The thermal stability behaviors of all samples were further studied by the DSC. The incorporation of nanoclay into the polymer matrix did not only affect the degradation temperature but also influenced the glass transition temperature (T_g). Figure 6d displays the DSC analysis of all samples and their corresponding T_g values were obtained from the second heating process. As can be seen from Figure 6d, an appreciable reduction of T_g was noticed for all samples in comparison with the neat PPC polyol. The T_g of −3.0, −18.0, −30.0, and −40.0 °C were obtained for the MMT nanoclay content of 0.0, 1.0, 2.0, and 4.0 wt %, respectively.

The thermal properties of the polymer nanocomposites may be enhanced or deteriorated depending on the chemical nature of the polymer matrix or filler, as well as the polymer−filler interactions. In our study, the results showed that the thermal stability of all nanocomposite samples decreased in the presence of the nanoclay and the level of nanoclay loading remarkably influenced the thermal degradation as well as T_g. The reduced thermal stability could be attributed to the effect of well-dispersed nanoclay as well as fully exfoliated nanoclay lamella in the polymer matrix. The high surface area of the nanoclay layers per unit volume of polymer matrix leads to a higher dispersion of nanoclay lamella.

The high degree of dispersion of well-exfoliated nanoclay lamella has been shown to lower the T_g, especially at a lower nanoclay content. This result was unexpected since previous reports in the literature showed that with a high molecular weight PPC nanocomposite, the thermal stability was improved markedly with nanoclay loading.[49] Our results imply that the nanocomposites prepared in the present study having a fully exfoliated structure are more pronounced of lowering the thermal stability than those of the nanocomposites containing only intercalated nanoclay stacks.

Another factor that may contribute to the reduction in the thermal stability is the plasticizing effect of the nanoclay. Through the exfoliation phenomena, the nanoclay acts as a plasticizer to embed nanoclay lamellae into the polymeric chains causing a network breakup between the nanoclay and the polymer. Of course, the effect is more pronounced with more loading due to the large surface area of the lamellae generated from the nanoclay.[49] As a result, the change in molecular dynamics causes the thermal stability (i.e., T_g) of polymer nanocomposites to reduce.

Because the T_g is also influenced by the surface property of the nanoclay, the hydrophobic chain ends may suppress the interaction with the filler surface, creating more defect/free at the nanoclay/polymer chain interface. This will certainly

https://doi.org/10.1021/acsomega.2c05705
ACS Omega 2023, 8, 5247−5256

reduce the T_g as the chain end contribution per molecule is dominant particularly at a low molecular weight. However, at a high molecular weight, for the same polymer, a slight increase or negligible influence on T_g may be observed because the chain end contribution per molecule diminishes.[49]

The polymer nanocomposite was further analyzed by ^{1}H NMR to confirm that no major changes to chemical structure were associated with the nanoclay addition. Figure 7 illustrates the results of the polymer nanocomposites at different nanoclay contents.

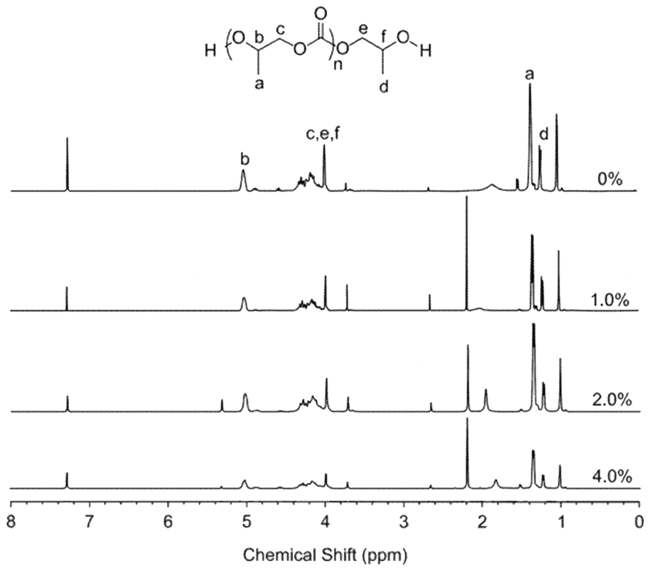

Figure 7. ^{1}H NMR spectrum of the neat PPC, PPC polyol, and their nanocomposites at different nanoclay concentrations.

As can be clearly seen from the ^{1}H NMR spectrum, we noticed additional signals at 2.2 and 5.3 ppm, which represent the methyl group originating from the exfoliation agent and the residual amounts of the solvent used, respectively. It was also observed that the addition of nanoclay had contributed to another additional peak intensity at 1.6 ppm. This is attributed to the formation of cyclic carbonate propylene (CPC), a decomposing product of PPC polyol. This was also observed at 1800 cm^{-1} in the FT-IR analysis shown in Figure 4. The degradation of polycarbonate molecules in the presence of nanoclay has been previously reported.[50] It was explained that the reinforced polycarbonate nanocomposite tends to be hydrolyzed in the presence of nanoclay. The hydrolysis of the polycarbonate chains will lead to a decrease in the polymer molecular weight; hence, lower the thermal stability.[51]

This was also confirmed by the molecular weight results obtained by MALDI–TOF MS (see Figure 8a–d). However, the effect of nanoclay addition has only contributed to a minor reduction in the molecular weight (Table 2). This suggests that the chemical structure of PPC polyol was effectively maintained during PPC nanocomposite preparation when an

Table 2. Comparison of the Average-Number Molecular Weight and Polydispersity Index, PDI, for Various Nanocomposites

nanoclay content, wt %	M_n, g mol^{-1} (GPC)	PDI	M_n, g mol^{-1} (MALDI–TOF MS)	PDI
0	1037	1.04	1103	1.0
1	1037	1.04	1050	1.0
2	890	1.05	1015	1.0
4	860	1.05	1058	1.0

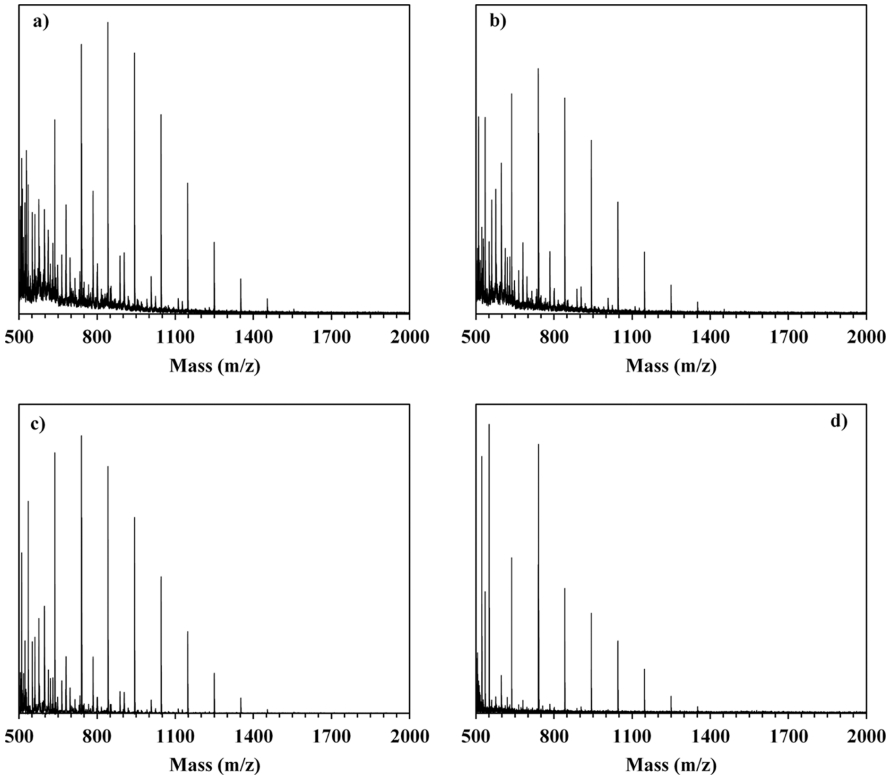

Figure 8. (a–d) MALDI–MS TOF of the neat PPC polyol, PPC, and their nanocomposites at different nanoclay contents.

https://doi.org/10.1021/acsomega.2c05705
ACS Omega 2023, 8, 5247–5256

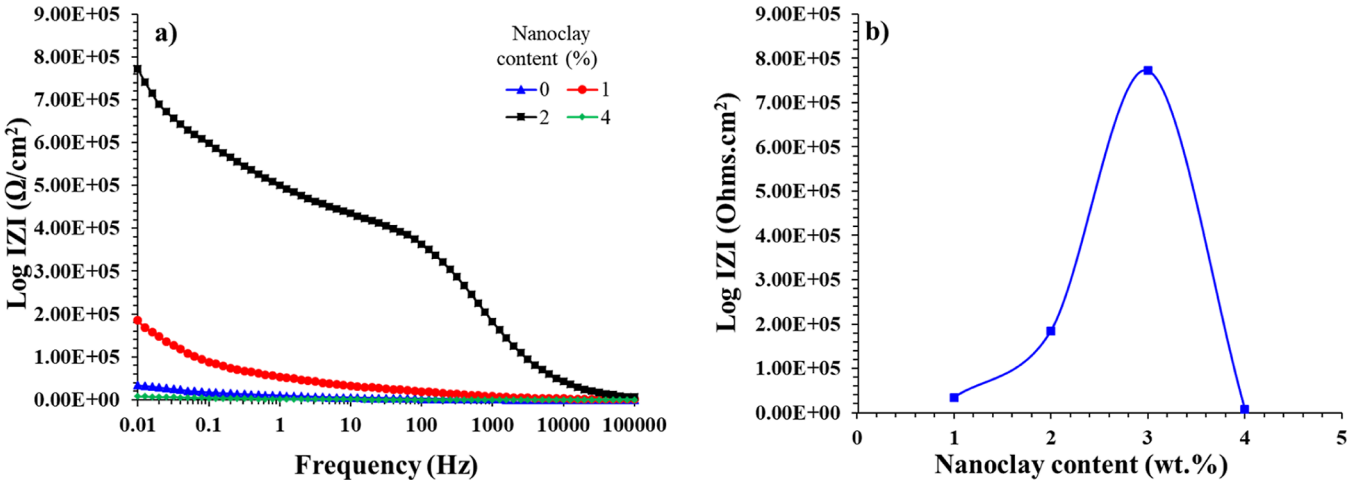

Figure 9. EIS: (a) bode plot of PPC nanocomposite-based PU at a range of 0.01 Hz to 100 kHz for 24 h, respectively. (b) PPC nanocomposite-based PU with different clay contents at 0.01 Hz.

optimum nanoclay concentration was achieved. At this concentration, the formation of cyclic propylene carbonate (CPC) has been minimized. This minimum or critical concentration was found to be 2.0 wt % for the current system. When 2.0 wt % or more nanoclay was added, however, a significant decrease in molecular weight was observed.

The developed PPC nanocomposite was extended to synthesize PU-based material for anticorrosion coating. It has been observed that during PU synthesis, the PPC nanocomposites with low viscosity exhibit a homogeneous mixture. This translated to a better processability and binding characteristics on the metal substrate. The analysis of the corrosion behavior of PPC nanocomposite-based PU was performed using an EIS technique for 24 h. EIS is a well-established quantitative method for the accelerated evaluation of the anti-corrosion characteristics and performance of protective coatings. The coating resistance (Z) expressed in Ω/cm^2 is a parameter for ion transport resistance through the coating, which is one of the most important factors in corrosion resistance.

Figure 9a shows the impedance response, Z measured at diverse frequencies for all samples, with similar variations. The figure appeared to indicate the effectiveness of the anti-corrosive PPC nanocomposite-based PU coating with the addition of exfoliated nanoclay. The decrease of the impedance Z magnitude as the frequency increases corresponds to the fact that the corroded surface is capacitive in nature. It is clearly noticed that there is a strong correlation between the impedance Z response at different clay contents (see Figure 9b). This suggests that the PU coating from the PPC nanocomposite showed higher corrosion rates in comparison to only the PPC-based PU. It also an indication that the anticorrosion characteristics improved with clay addition, up to 2.0 wt %, for the current study. These results were attributed to the nanoscale structure and interfacial characteristics of the PPC nanocomposite-based PU, the robust, hydrophobic, and blocking nature of the carbonate coatings.[52,53] The nano-structured characteristics increase the length of the diffusion pathway by shielding the metal substrate (barrier protection) and hence decrease the permeability of the water and oxygen.[54,55]

CONCLUSIONS

In this study, nanocomposite of CO_2-based polycarbonate polyol with highly exfoliated nanoclay was successfully synthesized by solution intercalation. The incorporation of the nanoclay within the polymer matrix altered the polyol's physical properties. In particular, the nanoclay was functioned as a rheological agent for lowering the viscosity of the PPC polyol.

The concentrations of nanoclay showed the most significant impacts on the synthesis of the PPC nanocomposites. The viscosity decreased from 30000.0 to 300 cP for 0.0 and 4.0 wt % nanoclay content, respectively. However, increasing the nanoclay content beyond the critical concentration, C_{cri}, (~2.0 wt % for the current system) led to the depolymerization of PPC. This was indicated by the formation of the cyclic propylene carbonate (CPC). The PPC nanocomposites with low viscosity were used as a precursor to make PU-based coating materials. The formation and processability during the PU synthesis were more homogeneous due to the improved viscosity of PPC. The PU coating derived from the PPC nanocomposite exhibited higher anticorrosion coating properties in comparison to the non-modified PU coating.

AUTHOR INFORMATION

Corresponding Author

Mohammad Alroaithi − *Fuel & Chemicals, Aramco Research Center, King Abdullah University of Science and Technology, Thuwal 23955-8433, Kingdom of Saudi Arabia;* orcid.org/0000-0003-1488-8189; Email: Mohammad.alroaithi@aramco.com

Author

Wei Xu − *Fuel & Chemicals, Aramco Research Center, King Abdullah University of Science and Technology, Thuwal 23955-8433, Kingdom of Saudi Arabia*

Complete contact information is available at: https://pubs.acs.org/10.1021/acsomega.2c05705

Notes

The authors declare no competing financial interest.

https://doi.org/10.1021/acsomega.2c05705
ACS Omega 2023, 8, 5247−5256

■ ACKNOWLEDGMENTS

The authors would like to acknowledge the financial support provided by Aramco Research Center.

■ REFERENCES

(1) Appel, A.; Bercaw, J.; Bocarsly, A.; Dobbek, H.; DuBois, D.; Dupuis, M.; Ferry, J.; Fujita, E.; Hille, R.; Kenis, P.; et al. Frontiers, opportunities, and challenges in biochemical and chemical catalysis of CO2 fixation. *Chem. Rev.* **2013**, *113*, 6621−6658.
(2) Mikkelsen, M.; Jørgensen, M.; Krebs, F. C. The teraton challenge. A review of fixation and transformation of carbon dioxide. *Energy Environ. Sci.* **2010**, *3*, 43−81.
(3) Sakakura, T.; Choi, J. C.; Yasuda, H. Transformation of carbon dioxide. *Chem. Rev.* **2007**, *107*, 2365−2387.
(4) Stępak, B.; Antończak, A. J.; Bartkowiak-Jowsa, M.; Filipiak, J.; Pezowicz, C.; Abramski, K. M. Fabrication of a polymer-based biodegradable stent using a CO2 laser. *Arch. Civ. Mech. Eng.* **2014**, *14*, 317−326.
(5) Cuéllar-Franca, R. M.; Azapagic, A. Carbon capture, storage and utilisation technologies: A critical analysis and comparison of their life cycle environmental impacts. *J. CO2 Util.* **2015**, *9*, 82−102.
(6) Kember, M. R.; Buchard, A.; Williams, C. K. Catalysts for CO 2/epoxide copolymerisation. *Chem. Commun.* **2011**, *47*, 141−163.
(7) Qin, Y.; Sheng, X.; Liu, S.; Ren, G.; Wang, X.; Wang, F. Recent advances in carbon dioxide-based copolymers. *J. CO2 Util.* **2015**, *11*, 3−9.
(8) Muthuraj, R.; Mekonnen, T. Recent progress in carbon dioxide (CO2) as feedstock for sustainable materials development: Co-polymers and polymer blends. *Polym. J.* **2018**, *145*, 348−373.
(9) Chisholm, M. H.; Navarro-Llobet, D.; Zhou, Z. Poly (propylene carbonate). 1. More about poly (propylene carbonate) formed from the copolymerization of propylene oxide and carbon dioxide employing a zinc glutarate catalyst. *Macromolecules* **2002**, *35*, 6494−6504.
(10) Darensbourg, D. J.; Holtcamp, M. W. Catalysts for the reactions of epoxides and carbon dioxide. *Coord. Chem. Rev.* **1996**, *153*, 155−174.
(11) Li, X.; Meng, L.; Zhang, Y.; Qin, Z.; Meng, L.; Li, C.; Liu, M. Research and Application of Polypropylene Carbonate Composite Materials: A Review. *Polym. J.* **2022**, *14*, 2159.
(12) Roudsari, G. M.; Mohanty, A. K.; Misra, M. Exploring the effect of poly (propylene carbonate) polyol in a biobased epoxy interpenetrating network. *ACS Omega* **2017**, *2*, 611−617.
(13) von der Assen, N.; Bardow, A. Life cycle assessment of polyols for polyurethane production using CO 2 as feedstock: insights from an industrial case study. *Green Chem.* **2014**, *16*, 3272−3280.
(14) Alagi, P.; Ghorpade, R.; Choi, Y. J.; Patil, U.; Kim, I.; Baik, J. H.; Hong, S. C. Carbon dioxide-based polyols as sustainable feedstock of thermoplastic polyurethane for corrosion-resistant metal coating. *ACS Sustain. Chem. Eng.* **2017**, *5*, 3871−3881.
(15) Luinstra, G. A. Poly (propylene carbonate), old copolymers of propylene oxide and carbon dioxide with new interests: catalysis and material properties. *Polym. Eng. Rev.* **2008**, *48*, 192−219.
(16) Nair, K. M.; Thomas, S. Effect of interface modification on the mechanical properties of polystyrene-sisal fiber composites. *Polym. Compos.* **2003**, *24*, 332−343.
(17) Tang, L. G.; Kardos, J. L. A review of methods for improving the interfacial adhesion between carbon fiber and polymer matrix. *Polym. Compos.* **1997**, *18*, 100−113.
(18) Rout, J.; Misra, M.; Tripathy, S. S.; Nayak, S. K.; Mohanty, A. K. The influence of fibre treatment on the performance of coir-polyester composites. *Compos. Sci. Technol.* **2001**, *61*, 1303−1310.
(19) George, M.; Chae, M.; Bressler, D. C. Composite materials with bast fibres: Structural, technical, and environmental properties. *Prog. Mater. Sci.* **2016**, *83*, 1−23.
(20) Muthuraj, R.; Misra, M.; Mohanty, A. K. Biocomposite consisting of miscanthus fiber and biodegradable binary blend matrix: Compatibilization and performance evaluation. *RSC Adv.* **2017**, *7*, 27538−27548.
(21) Guo, F.; Aryana, S.; Han, Y.; Jiao, Y. A Review of the Synthesis and Applications of Polymer-Nanoclay Composites. *Appl. Sci.* **2018**, *8*, 1696.
(22) Usuki, A.; Hasegawa, N.; Kato, M.; Kobayashi, S. Polymer-clay nanocomposites. *Polym. Compos.* **2005**, 135−195.
(23) Zhang, Y.; Choi, J. R.; Park, S. J. Interlayer polymerization in amine-terminated macromolecular chain-grafted expanded graphite for fabricating highly thermal conductive and physically strong thermoset composites for thermal management applications. *Compos. Appl. Sci. Manuf.* **2018**, *109*, 498−506.
(24) Thakur, V. K.; Kessler, M. R. Self-healing polymer nanocomposite materials: A review. *Polym. J.* **2015**, *69*, 369−383.
(25) Maiti, M.; Bhowmick, A. K. New fluoroelastomer nanocomposites from synthetic montmorillonite. *Compos. Sci. Technol.* **2008**, *68*, 1−9.
(26) Ozkose, U. U.; Altinkok, C.; Yilmaz, O.; Alpturk, O.; Tasdelen, M. A. In-situ preparation of poly (2-ethyl-2-oxazoline)/clay nanocomposites via living cationic ring-opening polymerization. *Eur. Polym. J.* **2017**, *88*, 586−593.
(27) Karamane, M.; Raihane, M.; Tasdelen, M. A.; Uyar, T.; Lahcini, M.; Ilsouk, M.; Yagci, Y. Preparation of fluorinated methacrylate/clay nanocomposite via in-situ polymerization: Characterization, structure, and properties. *J. Polym. Sci., Part A: Polym. Chem.* **2017**, *55*, 411−418.
(28) Guo, F.; Aryana, S.; Han, Y.; Jiao, Y. A review of the synthesis and applications of polymer−nanoclay composites. *Appl. Sci.* **2018**, *8*, 1696.
(29) Yin, J.; Deng, B. Polymer-matrix nanocomposite membranes for water treatment. *J. Membr. Sci.* **2015**, *479*, 256−275.
(30) Melia, M. A.; Percival, S. J.; Qin, S.; Barrick, E.; Spoerke, E.; Grunlan, J.; Schindelholz, E. J. Influence of Clay size on corrosion protection by Clay nanocomposite thin films. *Prog. Org. Coat.* **2020**, *140*, 105489.
(31) Viseras, C.; Cerezo, P.; Sanchez, R.; Salcedo, I.; Aguzzi, C. Current challenges in clay minerals for drug delivery. *Appl. Clay Sci.* **2010**, *48*, 291−295.
(32) Alhwaige, A. A.; Ishida, H.; Qutubuddin, S. Carbon aerogels with excellent CO2 adsorption capacity synthesized from clay-reinforced biobased chitosan-polybenzoxazine nanocomposites. *ACS Sustain. Chem. Eng.* **2016**, *4*, 1286−1295.
(33) Unuabonah, E. I.; Günter, C.; Weber, J.; Lubahn, S.; Taubert, A. Hybrid clay: a new highly efficient adsorbent for water treatment. *ACS Sustain. Chem. Eng.* **2013**, *1*, 966−973.
(34) Wu, Z.; Zhang, P.; Zhang, H.; Li, X.; He, Y.; Qin, P.; Yang, C. Tough porous nanocomposite hydrogel for water treatment. *J. Hazard. Mater.* **2022**, *421*, 126754.
(35) Bee, S. L.; Abdullah, M. A. A.; Bee, S. T.; Sin, L. T.; Rahmat, A. R. Polymer nanocomposites based on silylated-montmorillonite: A review. *Prog. Polym. Sci.* **2018**, *85*, 57−82.
(36) Abdelraheem, A.; El-Shazly, A. H.; Elkady, M. F. Synthesis and characterization of intercalated polyaniline-clay nanocomposite using supercritical CO2. *AIP Conf. Proc.* **2018**, *1*, 020027.
(37) Utracki, L. A.*Clay-containing polymeric nanocomposites*; iSmithers Rapra Publishing, 2004; Vol. *1*.
(38) Saba, N.; Jawaid, M.; Asim, M. Recent advances in nanoclay/natural fibers hybrid composites. *Polym. Compos.* **2016**, 1−28.
(39) Shen, Z.; Simon, G. P.; Cheng, Y. B. Comparison of solution intercalation and melt intercalation of polymer−clay nanocomposites. *Polym. J.* **2002**, *43*, 4251−4260.
(40) Le Pluart, L. D. J. S. H.; Duchet, J.; Sautereau, H.; Gérard, J. F. Surface modifications of montmorillonite for tailored interfaces in nanocomposites. *J. Adhes.* **2002**, *78*, 645−662.
(41) Shi, X.; Gan, Z. Preparation and characterization of poly (propylene carbonate)/montmorillonite nanocomposites by solution intercalation. *Eur. Polym. J.* **2007**, *43*, 4852−4858.

https://doi.org/10.1021/acsomega.2c05705
ACS Omega 2023, 8, 5247−5256

(42) Anandhan, S.; Patil, H. G.; Babu, R. R. Characterization of poly (ethylene-co-vinyl acetate-co-carbon monoxide)/layered silicate clay hybrids obtained by melt mixing. *J. Mater. Sci.* **2011**, *46*, 7423−7430.
(43) Kader, M. A.; Bhowmick, A. K. Thermal ageing, degradation and swelling of acrylate rubber, fluororubber and their blends containing polyfunctional acrylates. *Polym. Degrad. Stab.* **2003**, *79*, 283−295.
(44) Alagi, P.; Ghorpade, R.; Choi, Y. J.; Patil, U.; Kim, I.; Baik, J. H.; Hong, S. C. Carbon dioxide-based polyols as sustainable feedstock of thermoplastic polyurethane for corrosion-resistant metal coating. *ACS Sustain. Chem. Eng.* **2017**, *5*, 3871−3881.
(45) La Mantia, F. P.; Scaffaro, R.; Ceraulo, M.; Mistretta, M. C.; Dintcheva, N. T.; Botta, L. A simple method to interpret the rheological behaviour of intercalated polymer nanocomposites. *Compos. B Eng.* **2016**, *98*, 382−388.
(46) Dorigato, A.; Pegoretti, A.; Penati, A. Linear low-density polyethylene/silica micro-and nanocomposites: dynamic rheological measurements and modelling. *Express Polym. Lett.* **2010**, *4*, 115−129.
(47) Yeganeh, J. K.; Goharpey, F.; Moghimi, E.; Petekidis, G.; Foudazi, R. Controlling the kinetics of viscoelastic phase separation through self-assembly of spherical nanoparticles or block copolymers. *Soft Matter* **2014**, *10*, 9270−9280.
(48) Jain, S.; Goossens, J. G.; Peters, G. W.; van Duin, M.; Lemstra, P. J. Strong decrease in viscosity of nanoparticle-filled polymer melts through selective adsorption. *Soft Matter* **2008**, *4*, 1848−1854.
(49) Zare, Y.; Rhee, K. Y. Dependence of Z parameter for tensile strength of multi-layered interphase in polymer nanocomposites to material and interphase properties. *Nanoscale Res. Lett.* **2017**, *12*, 1−7.
(50) Liu, B. H.; Zhang, M.; Yu, A. F.; Chen, L. B. Degradation mechanism of poly (propylene carbonate) polyols. *Polym. Mater.: Sci. Eng.* **2004**, *20*, 76−79.
(51) Cui, L.; Bara, J. E.; Brun, Y.; Yoo, Y.; Yoon, P. J.; Paul, D. R. Polyamide-and polycarbonate-based nanocomposites prepared from thermally stable imidazolium organoclay. *Polym. J.* **2009**, *50*, 2492−2502.
(52) Pathan, S.; Ahmad, S. Synthesis, characterization and the effect of the s-triazine ring on physico-mechanical and electrochemical corrosion resistance performance of waterborne castor oil alkyd. *J. Mater. Chem. A.* **2013**, *1*, 14227−14238.
(53) Mathai, S.; Shaji, P. S. Polymer-Based Nanocomposite Coating Methods: A Review. *J. Sci. Res.* **2022**, *14*, 973−1002.
(54) Olad, A.; Rashidzadeh, A. Preparation and anticorrosive properties of PANI/Na-MMT and PANI/O-MMT nanocomposites. *Prog. Org. Coat.* **2008**, *62*, 293−298.
(55) Abu-Thabit, N. Y.; Makhlouf, A. S. H.Recent advances in nanocomposite coatings for corrosion protection applications. *Handbook of nanoceramic and nanocomposite coatings and materials*; Elsevier, 2015; pp 515−549.

https://doi.org/10.1021/acsomega.2c05705
ACS Omega 2023, 8, 5247−5256